Numerical study of discrete Lorenz-like attractors.

Kazakov A.[1], Murillo A.[2], Vieiro A.[2,3] and Zaichikov K.[1]

[1] National Research University Higher School of Economics,

25/12 Bolshaya Pecherskaya Ulitsa, 603155 Nizhny Novgorod, Russia

kazakovdz@yandex.ru, zaychikovkirill3@gmail.com

[2] Departament de Matemàtiques i Informàtica, Universitat de Barcelona,

Gran Via de les Corts Catalanes, 585, 08007 Barcelona, Spain

[3] Centre de Recerca Matemàtica (CRM), 08193 Bellaterra, Spain

amurillo@ub.edu, vieiro@ub.edu

January 22, 2024

Abstract

We consider a homotopic to the identity family of maps, obtained as a discretization of the Lorenz system, such that the dynamics of the last is recovered as a limit dynamics when the discretization parameter tends to zero. We investigate the structure of the discrete Lorenz-like attractors that the map shows for different values of parameters. In particular, we check the pseudohyperbolicity of the observed discrete attractors and show how to use interpolating vector fields to compute kneading diagrams for near-the-identity maps. For larger discretization parameter values, the map exhibits what appears to be genuinely-discrete Lorenz-like attractors, that is, discrete chaotic pseudohyperbolic attractors with a negative second Lyapunov exponent. The numerical methods used are general enough to be adapted for arbitrary near-identity discrete systems with similar phase space structure.

Keywords. Lorenz attractor, pseudohyperbolicity, interpolating vector fields, kneading diagrams.

1 Introduction

The Lorenz attractor is one of the first, well-known, and extensively studied chaotic attractors. It is observed in various contexts, including hydrodynamical models [40, 43, 55, 62], optical systems [52, 53], normal forms for certain classes of local bifurcations [30, 51, 58]; its discrete analogues are found in nonholonomic dynamics [22, 24], convection systems [15, 16], normal forms for some types of homoclinic bifurcations [32], etc.

There are several, and not completely equivalent, definitions of the Lorenz attractor. Most of them are based on geometric ideas. Classical definitions go back to the Guckenheimer-Williams [36, 37, 65] and Afraimovich-Bykov-Shilnikov [1, 2] geometric models; their generalizations can be found in [5, 49]. For the Lorenz attractor, we will use the definition based on the pseudohyperbolicity notion, see details in Section 2.

Pseudohyperbolicity – a weak version of hyperbolicity – is one of the main features of the Lorenz attractor. The foundations of the theory of pseudohyperbolic attractors were laid in [63]. The common property of pseudohyperbolic attractors is the existence of a continuous splitting of the tangent space in a neighborhood of an attractor into a direct sum of two invariant linear subspaces E^{ss} and E^{cu}: the linearized system restricted to E^{ss} is uniformly contracting, whereas in E^{cu} it uniformly expands volumes. In the case of hyperbolic attractors, the field of subspaces E^{cu} is given by tangents to the unstable manifolds. In the case of pseudohyperbolicity, the linearized system can contract some directions in E^{cu}, however, the total volume expansion in this subspace ensures that the maximal Lyapunov exponent for every orbit of the attractor is always positive. The fact that any possible contraction in E^{cu} must be uniformly weaker than any contraction in E^{ss}, guarantees the positivity of the maximal Lyapunov exponent for all orbits in the attractor and that this property is preserved at small perturbations of the system. In other words, the pseudohyperbolicity of an attractor means that this attractor is robustly chaotic.

The current work is devoted to the study of a discrete analogue of the Lorenz attractor – the so-called *discrete Lorenz attractor*. We will give its definition in Section 2; here we would like to underline that as the classical Lorenz attractor, its discrete analogue is also pseudohyperbolic. Let us start with some history. The first example of the discrete Lorenz attractor was found in [32] in the 3D Hénon map

$$\begin{cases} \bar{x} = y, \\ \bar{y} = z, \\ \bar{z} = M_1 + Bx + M_2 z - z^2. \end{cases} \tag{1}$$

with parameters M_1, M_2, and B. An example of this attractor is shown in Fig. 1a. In [32], it was also proved that such attractors appear near the codimension three bifurcation when a fixed point of the map has multipliers $(-1, -1, 1)$. The reason for its birth is that the asymptotic normal form for this bifurcation is the Shimizu-Morioka system of three differential equations. The existence of the Lorenz attractors for this system is a known fact [56, 57, 59] proved in [12]. However for the 3D Hénon map the discrete Lorenz attractors were observed in [32] quite far from the codimension three point, where the theory of asymptotic normal forms does not work. Their pseudohyperbolicity was numerically confirmed recently in [25, 31].

Discrete Lorenz attractors are also observed in applications. Their first example was found in the nonholonomic model of Celtic stone [22], and considerations in favor of its

pseudohyperbolicity were provided in [23]. Also, such attractors are observed in convection systems [15, 16]. As we know, there are currently no rigorous results confirming the pseudohyperbolicity of these discrete Lorenz attractors.

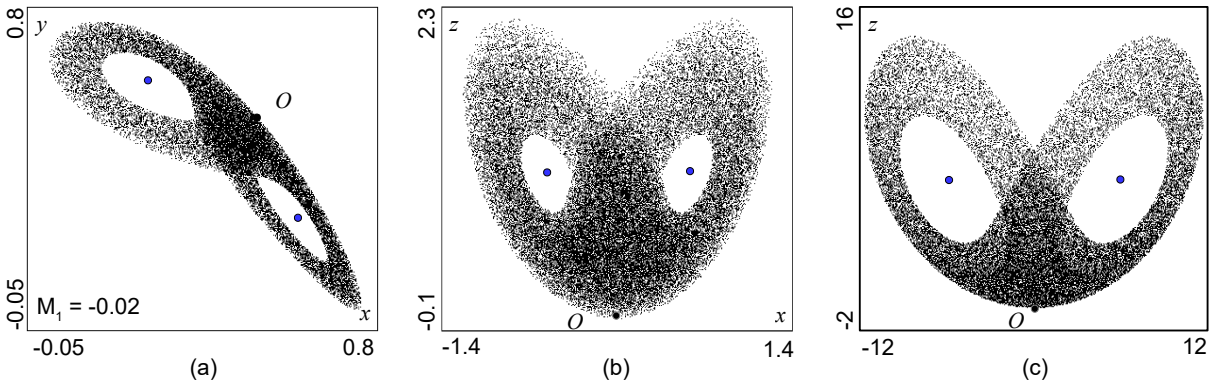

Figure 1: Examples of discrete Lorenz attractors in: (a) the three-dimensional Hénon map (1) at $(B, M_1, M_2) = (0.7, -0.02, 0.85)$; (b) periodically perturbed Shimizu-Morioka system (2) at $(\alpha, \lambda, \varepsilon) = (0.35, 0.9, 0.01)$; (c) map (4) at $(\rho, \sigma, b, \delta) = (8, 4, 8/3, 0.1)$.

In the paper by Turaev and Shilnikov [64] it was proved that pseudohyperbolic properties of the Lorenz attractor persist under small periodic perturbations of the system. For the perturbed system, on the Poincaré map for the period, the attractor looks like the Lorenz attractor observed in the 3D Hénon map. An illustration of this result can be found in [29] where the discrete Lorenz attractor was found and studied in the periodically perturbed Shimizu-Morioka system

$$\begin{cases} \dot{x} = y, \\ \dot{y} = x - \lambda y - xz, \\ \dot{z} = -\alpha z + x^2 + \varepsilon z \sin t, \end{cases} \tag{2}$$

with parameters α, λ, and ε. The Poincaré map for the attractor existing at $\alpha = 0.35, \lambda = 0.9$, and $\varepsilon = 0.01$ is shown in Fig. 1b.

In this paper, we use another scheme to obtain a family of maps that exhibit discrete Lorenz attractors. We take a system of differential equations with the Lorenz attractor and apply a semi-implicit Euler integration step to obtain a discrete map. Concretely, as the basic system we consider the Lorenz model [40]

$$\begin{cases} \dot{x} = \sigma(y - x), \\ \dot{y} = x(\rho - z) - y, \\ \dot{z} = xy - \beta z, \end{cases} \tag{3}$$

with parameters $\beta = 8/3, \sigma$, and ρ. After applying an integration step we obtain the following map

$$\begin{cases} \bar{x} = x + \delta(\sigma(y - x)), \\ \bar{y} = y + \delta(\bar{x}(\rho - z) - y), \\ \bar{z} = z + \delta(\bar{x}y - \beta z). \end{cases} \tag{4}$$

with the same parameters β, σ, and ρ and integration step δ. When $\delta \to 0$ the dynamics of the map resembles that of the Lorenz system. Moreover, for δ small enough the map

(4) becomes a near-the-identity map, then it can be formally embedded into a 3D time-periodic flow (a suspension) defined in a suitable topological manifold. The map (4) is then exactly recovered as the period-map of the suspension flow. The setting is then analogous to that in [64], then discrete Lorenz-like attractors are expected for δ small enough. An example of an attractor in the map (4) is shown in Fig. 1c.

With the help of the toy-map (4), we try to understand the nature and properties of discrete Lorenz attractors. For this aim, we:

- apply the Lyapunov analysis and angle's methods for the verification of pseudohyperbolicity conditions;
- adapt the so-called kneading invariant for the maps using interpolating vector fields method;
- compare, for δ small, the numerical results of pseudohyperbolicity verification with those obtained by a direct investigation of the one-dimensional return map which we compute using the Poincaré map constructed from the interpolating vector field.

In [32], for the map (1), it was noted that visually similar Lorenz attractors populate an open large region in the (M_1, M_2)-parameter plane. This region is characterized by the following signature of Lyapunov exponents $\Lambda_1 > \Lambda_2 > \Lambda_3$:

$$\Lambda_1 > 0,\ \Lambda_2 \approx 0,\ \Lambda_3 < 0.$$

In other words, chaotic attractors in this region have a "flow" nature, since (as in any 3D flow system exhibiting a chaotic pseudohyperbolic attractor) they have a second Lyapunov exponent Λ_2 indistinguishable from zero. At first, for our toy map (4) we compute Lyapunov diagrams on the (ρ, σ)-parameter plane for different values of the step parameter δ, see Fig. 3. It is interesting to note that we observe large regions with chaotic attractors with a second Lyapunov exponent close to zero even for sufficiently large values of δ.

After this, we verify the pseudohyperbolicity of attractors in the map (4) on the same parameter planes. For this, we apply the so-called *angle's method* suggested in [38, 39]. We start with the classical Lorenz model (3) (which is the limit for $\delta \to 0$ in the map (4)) and, at first, reproduce known results of the localization of the Lorenz attractor existence region obtained early in [10, 11, 13] via verification of the Afraimovich-Bykov-Shilnikov conditions [1, 2]. Then, we apply the angle's method for pseudohyperbolicity verification to the map (4) for $\delta > 0$. We found that pseudohyperbolicity of chaotic attractors persists even for sufficiently large values of δ, see Fig. 4. It is worth noting that $\Lambda_2 \approx 0$ in most regions with pseudohyperbolic attractors (the regions I, II, and III in Fig. 4d); these parameter values correspond to the so-called *flow-like discrete pseudohyperbolic Lorenz attractors*. However, we also found attractors of another nature, for which Λ_2 is clearly separated from 0. Such attractors populate the region IV in Fig. 4d, we call them *genuinely discrete pseudohyperbolic Lorenz attractors*. As far as we know, such attractors were not previously observed.

Despite the visual similarity of the Lorenz attractors of 3D flows and their discrete analogues in 3D maps, they differ fundamentally. Pseudohyperbolicity prevents homoclinic (and heteroclinic) tangencies in 3D flows, i.e., stable and unstable manifolds of

periodic saddle orbits in such systems intersect only transversally.[1] But in 3D maps there are classes of homoclinic tangencies (the so-called simple homoclinic tangencies) between invariant manifolds of saddle fixed/periodic orbits whose codimension one bifurcations generically do not produce stable periodic orbits [26, 27, 33, 35, 61]. Bifurcations of such tangencies produce a *wild hyperbolic set* [27, 50] – uniformly hyperbolic closed invariant set which always has a pair of saddle orbits such that the stable manifold of one orbit has a nontransversal intersection with the unstable manifold of another one, and this property is preserved for small perturbations. Such a set can be part of a pseudohyperbolic attractor. In this case we have a *wild pseudohyperbolic attractor*.

In the second part of the paper, we give numerical evidence that the pseudohyperbolic attractors in the map (4) for $\delta > 0$ are wild (see related comments in Section 4.3). To understand the abundance of homoclinic tangencies we apply interpolating vector fields [19] for recovering a flow from the map. Then, we use kneading diagrams [4, 66] which helped to understand the organization of homoclinic bifurcations in systems with Lorenz-like attractors.

The so-called interpolating vector fields (IVFs) were introduced in [19] to explore the dynamics of near-the-identity maps. At any point in the phase space, one evaluates a vector field by taking the derivative of the polynomial that interpolates some iterates of the map. For an optimal choice of the number of iterates, such a vector field gives an embedding of the map into an autonomous flow (of the same dimension as the map) with a small error, provided the map is close enough to the identity in the region of interest. This property is a consequence of the relation of IVFs with the discrete averaging method. In other words, IVFs are vector fields with analogous properties to the vector field obtained after removing the time-dependence of the suspension time-periodic flow to a suitable order (the order is related to the number of iterates used to construct the IVF and the closeness of the map to the identity). In particular, the dynamics of an IVF is expected to be simpler than the one of the map.

Indeed, from a practical point of view, IVFs can be used to reduce the complexity of the discrete system and obtain proper visualizations of the dynamics, see e.g. [19]. Furthermore, they do not rely on changes of coordinates, making IVFs computationally efficient and useful for global explorations of phase space dynamics as long as the map remains close-to-identity in the region explored.

In Section 4, we use IVFs to adapt some numerical methods to explore pseudohyperbolic attractors for a discrete map and illustrate them for the map (4). In particular, we show what happens with the homoclinic structures (homoclinic and multi-round homoclinic butterflies) when we use IVFs to approximate the dynamics. Then we compute kneading diagrams for different values of δ and compare them with the kneading diagram for the Lorenz system. The main bifurcation curves related to changes in the first symbols of the kneading sequence are displayed for different values of δ and allow to identify parameter regions where the discrete and flow attractors are similar (at least for δ small).

Finally, in Section 5, we use IVFs to project the iterates of the map (4) onto a transversal hyperplane, i.e., to obtain iterates of a 2D Poincaré return map from the 3D iterates of the original map. As expected, the strong normal hyperbolicity properties of the family of maps considered (recall that it is a discretization of the Lorenz flow) make the iterates of the Poincaré map behave similarly to a one-dimensional tent map. We use this fact

[1] In 3D flow systems bifurcations of homoclinic tangencies inevitably lead to the appearance of stable periodic orbits [17, 18], thus, an attractor cannot be pseudohyperbolic, in principle.

in an independent check (without relying on the angle between the Lyapunov vectors) of the pseudohyperbolicity properties of the observed attractors for small enough values of δ.

2 Main definitions: pseudohyperbolicity, Lorenz and discrete Lorenz attractors

Let $\mathcal{F}$ be a dynamical system defined on $\mathbb{R}^n$ and denote by F_t the time-t map of the evolution process. As usual, $t \in \mathbb{R}$ for continuous-time flow systems (hence F_t denotes the flow), while for a system defined by a diffeomorphism f consider $t \in \mathbb{Z}$ (and $F_t = f^t$). For our purposes, an attractor $\mathcal{A}$ of the system $\mathcal{F}$ is a minimal invariant set that attracts an open set of initial conditions. A chaotic attractor is an attractor such that the trajectories on it exhibit sensitivity with respect to initial conditions. Let us recall other more specific definitions used in this paper.

Definition 1 *[25, 31]. An attractor $\mathcal{A}$ is called pseudohyperbolic if the following properties hold for all $t \geq 0$ and all $x \in \mathcal{A}$:*

(a) *There exist two families of linear subspaces, $E_1(x)$ with $\dim E_1 = k$ and $E_2(x)$ with $\dim E_2 = n - k$, continuously dependent on x, which define an invariant splitting of the tangent space, i.e., $T_xM = E_1(x) \oplus E_2(x)$ with $DF_tE_i(x) = E_i(F_t(x))$, $i = 1, 2$.*

(b) *The splitting to E_1 and E_2 is dominated, i.e., there exist constants $C_1 > 0$ and $\beta > 0$ such that* [2]
$$\|DF_t(x)|_{E_2}\| \cdot \|(DF_t(x)|_{E_1})^{-1}\| \leq C_1 e^{-\beta t}$$

(c) *The differential DF restricted to E_1 exponentially expands all k-dimensional volumes, i.e., there exist constants $C_2 > 0$ and $\sigma > 0$ such that*
$$det(DF_t(x)|_{E_1}) \geq C_2 e^{\sigma t}$$

Similar to [34] we define,

Definition 2 *A (flow) Lorenz attractor is a pseudohyperbolic attractor of the Afraimovich-Bykov-Shilnikov geometrical Lorenz model given in [1, 2].*

Definition 3 *[29]. The discrete Lorenz attractor $\mathcal{A}$ is a pseudohyperbolic attractor such that:*

(i) it contains a saddle periodic point O with multipliers $\gamma, \lambda_1, \lambda_2, \ldots, \lambda_{n-1}$ such that $|\gamma| > 1$, $0 < |\lambda_{n-1}| \leq \cdots \leq |\lambda_2| < \lambda_1 < 1$, $|\lambda_1\lambda_2 \ldots \lambda_{n-1}\gamma| < 1$ and $\sigma \equiv |\lambda_1\gamma| > 1$;

(ii) it admits an adsorbing domain D having a pretzel shape (a ball with two handles);

[2] This condition means that any possible contraction in $E_1(x)$ is uniformly weaker than any contraction in $E_2(x)$, and any expansion in $E_1(x)$ is uniformly stronger than any possible expansion in $E_2(x)$. Note that it guarantees the persistence of the invariant families of linear subspaces E_1 and E_2 (and the attractor $\mathcal{A}$) under $\mathcal{C}^1$ perturbations of the system.

(iii) it contains the unstable separatrices Γ_1 *and* Γ_2 *(connected components of the set* $W^u(O)\backslash O$*);*

(iv) Γ_1 *leaves* O *and passes along one handle of the pretzel* D *and* Γ_2 *along the other handle;*

(v) all the homoclinic points of the intersections $\Gamma_1 \cap W^s_{loc}(O)$ *and* $\Gamma_2 \cap W^s_{loc}(O)$ *belong to the same half of* $W^s_{loc}(O)\backslash W^{ss}(O)$*, see Fig. 2.*

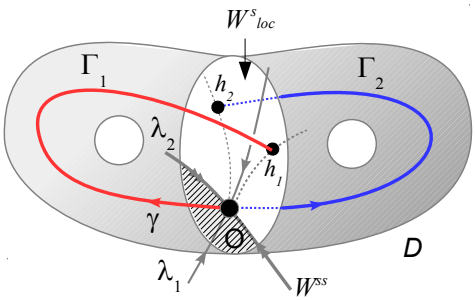

Figure 2: Illustration (from [29]) of the discrete Lorenz attractor according to the definition 3: D is an adsorbing domain (a ball with two handles); the curves $\Gamma_i \cup [h_i, O]$ are non-contractible in D; the homoclinic points h_1 and h_2 belong to the same part of $W^s_{loc}\backslash W^{ss}$.

Along the paper we will roughly distinguish two types of discrete Lorenz attractors, according to the following (empirical) criterion based on the computation of the second Lyapunov exponent:

- we will refer to such an attractor as "flow-like" if it is characterized by an indistinguishable from zero-second Lyapunov exponent $\Lambda_2 \approx 0$;
- we will refer to such an attractor as "genuinely-discrete" if it is characterized by a negative second Lyapunov exponent $\Lambda_2 < 0$.

In the current paper, we deal only with 3D systems. Therefore, $\dim(E_2) = 1$ and, since all vectors are contracted in E_2, it is convenient to use denotations E^{cu} and E^{ss} instead of E_1 and E_2, respectively, as we will do below.

3 Lyapunov analysis for the map (4)

In the first step, we compute Lyapunov diagrams for the map (4) on the (ρ, σ)-parameter plane for different values of the step parameter δ. We start with the limit case $\delta \to 0$ when this map degenerates to the classical Lorenz flow (3), and then increase δ. The resulting diagrams (computed on grids 1000×1000 on the parameter plane) are shown in Fig. 3. For the calculation of Lyapunov exponents $\Lambda_1 > \Lambda_2 > \Lambda_3$, we use the standard method suggested in [6]. At each pair of parameter values, we estimate the Lyapunov exponents integrating up to time $T = 10^6$ for the Lorenz flow (3) (Fig. 3a) and performing up to 10^6 iterates for the map (4) (Figs. 3b–3d). Depending on the values of Λ_i, the corresponding pixel of the diagram is colored according to the palette shown in the top-left corner of Fig. 3a.

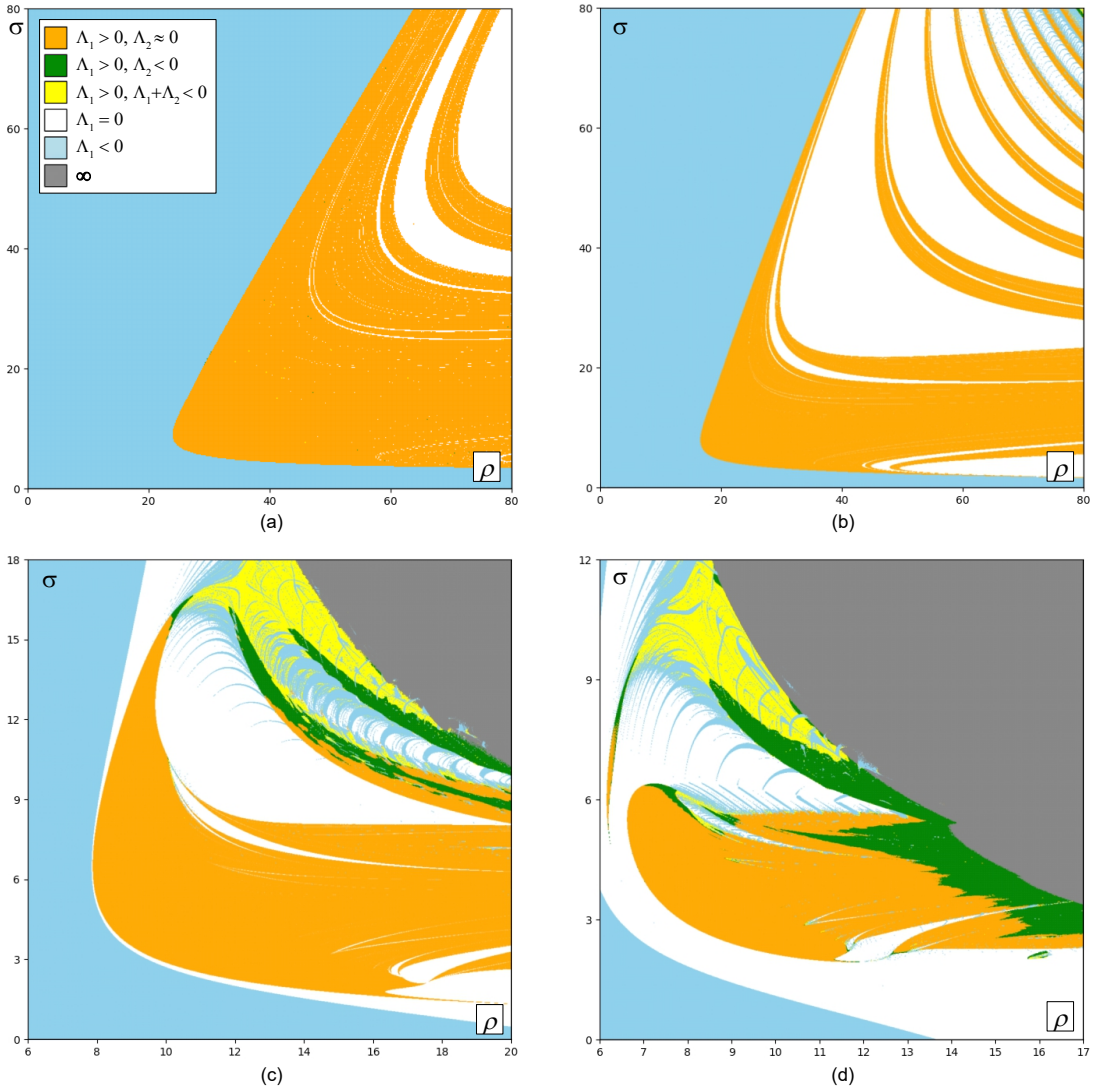

Figure 3: Lyapunov diagrams on the parameter plane (ρ, σ) for the (a) Lorenz system (3); (b)–(d) map (4) with (b) $\delta = 0.01$, (c) $\delta = 0.06$, (d) $\delta = 0.1$. Orange regions on these diagrams correspond to the "flow-like" attractors when $|\Lambda_2| < 0.001$; in the white regions the attractors have $|\Lambda_1| < 0.0001$; for parameters in the gray region, $W^u(O)$ is not bounded, see detailed color coding in the top-left corner of Fig. a.

On the one hand, Lyapunov diagrams in Fig. 3 show that the total size of the regions with chaotic attractors (i.e., with $\Lambda_1 > 0$) decreases as the parameter δ increases. On the other hand, one can see that there are orange-colored regions (with flow-like chaotic attractors) even for sufficiently large values of δ. We can argue that $\delta = 0.1$ can be considered as a large perturbation of the Lorenz flow, since the corresponding diagram is quite different from the diagram for the Lorenz flow, cf. Fig. 3d and Fig. 3a. Also, note that for δ not too small we detect regions with genuinely-discrete attractors (shown in green in Fig. 3c and Fig. 3d).

In the second step, we check the pseudohyperbolicity of chaotic attractors for the same values of the parameters as in Fig. 3. For this purpose, we apply the combination of methods proposed in [25, 31, 38, 39].

- At first, we verify the volume expanding condition $\Lambda_1 + \Lambda_2 > 0$, which prevents the

existence of stable periodic orbits inside the attractor. This condition, of course, holds for all chaotic attractors for the Lorenz flow (3). It also holds (at least with the resolution used for computations) for $\delta = 0.01$, but it is violated inside some regions (yellow-colored regions) with chaotic attractors for $\delta = 0.06$ and $\delta = 0.1$, see Figs. 3c and Figs. 3d.

- Then, we check the dominated splitting condition $\Lambda_2 > \Lambda_3$. In principle, this allows the decomposition of the tangent space at points of the attractor into invariant linear subspaces E^{ss} and E^{cu} with dimensions 1 and 2, respectively. Numerical experiments show that this condition is fulfilled for all chaotic attractors for the considered values of δ.

- Finally, we compute the minimal angle α_m between the subspaces E^{ss} and E^{cu}. The fulfillment of the condition $|\alpha_m| > 0$ guarantees the continuity of E^{ss} and E^{cu} with respect to the point in the attractor and, as a result, the persistence of chaoticity ($\Lambda_1 > 0$ for all orbits in the attractor) at small perturbations (changes in parameter values) of the system. We estimate the minimal angle using the method proposed in [38, 39], which allows us to compute the angle between the minimal covariant Lyapunov vector and the plane spanned by the other two covariant Lyapunov vectors. The resulting diagrams are presented in Fig. 4.

Remark 1 *The computation of the covariant Lyapunov vectors requires a long time forward and backward propagation of initial vectors along an orbit of an arbitrary point in the attractor. To avoid numerical errors, it is necessary to store the orbit iterates to follow them in the backward propagation. Note also that, for flows, the propagation requires the integration of the first variational equations. All this makes the computations cumbersome.*

Let us comment on the results presented in Fig. 4. As was shown in [10, 11], hyperbolicity of the attractor in the Lorenz flow (3) breaks down due to the appearance of a tangency between E^{ss} and E^{cu} along the unstable manifold $W^u(O)$. This tangency occurs on a codimension one manifold in the parameter space: on one side of this manifold, the attractor is pseudohyperbolic, while on the other side, cannot be pseudohyperbolic due to inevitable tangencies between E^{ss} and E^{cu}. On the (ρ, σ)-parameter plane, the corresponding curve l_A was also computed in [10, 11] and, in [13], this curve was further continued in the (ρ, σ)-parameter plane.

In Fig. 4a we reproduce part of these results computing the minimal angle between E^{ss} and E^{cu} along the unstable manifold $W^u(O)$. We take an initial point very close to the equilibrium O and integrate the system (3) up to time $T = 10^7$. If $|\alpha_m| < 0.001$ we display the corresponding pixel of the diagram in dark blue color. In Fig. 4a one can see positive angles beyond the curve l_A. This observation contradicts the theory in [10, 11], since beyond the curve l_A the minimal angle should vanish. We believe that increasing the integration time might improve the results but, unfortunately, computations become very time-consuming. In Section 5 we apply an alternative approach to check pseudohyperbolicity conditions.

After experiments with the Lorenz system, we compute diagrams of the minimal angle between E^{ss} and E^{cu} for the map (1). For $\delta = 0.01$ the corresponding diagram is shown in Fig. 4b. It slightly differs from the diagram computed for the Lorenz system.

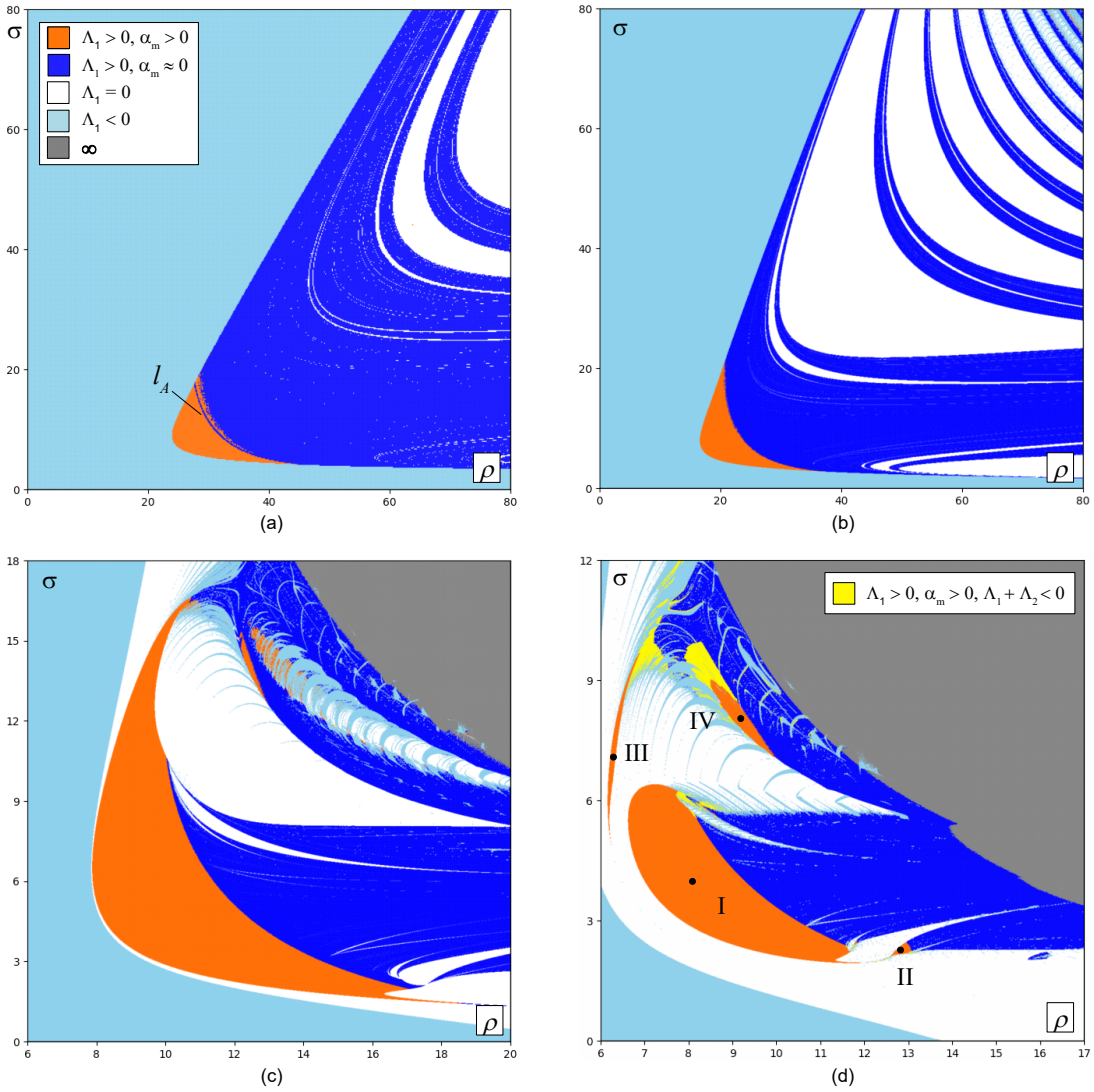

Figure 4: Minimal angle diagrams on the parameter plane (ρ, σ) for the (a) Lorenz system (3); (b)–(d) map (4) with (b) $\delta = 0.01$, (c) $\delta = 0.06$, (d) $\delta = 0.1$. In the blue-colored regions $|\alpha_m| < 0.001$. Within the corresponding region in panel (d) we detect parameters for which the attractor has $\Lambda_1 + \Lambda_2 < 0$, corresponding to the yellow-colored regions in Fig. 3, that cannot be pseudohyperbolic. In panel (a) we also display the curve l_A where the pseudohyperbolicity property of the (Lorenz) attractor is lost.

We observe that the size of the initial region with a Lorenz attractor decreases as δ increases, see Figs. 4c and 4d for $\delta = 0.06$ and $\delta = 0.1$, respectively. On the other side, for sufficiently large values of δ new regions with pseudohyperbolic attractors appear. This can be seen, for example, for $\delta = 0.1$ in Fig. 4d, where one detects four regions (I, II, III, and IV) with pseudohyperbolic attractors.

In the largest region I, inherited from the Lorenz system (3), $\Lambda_2 \approx 0$, i.e., attractors remain similar to the attractors of a three-dimensional autonomous Lorenz-like flow. The same is also true for attractors belonging to regions II and III which spawned from region I. On the other hand, in region IV we observe pseudohyperbolic attractors of another nature. Here $\Lambda_2 \in (-1.11, -0.06)$, i.e., it is clearly separated from zero. In contrast to flow-like Lorenz attractors, such attractors are genuinely-discrete attractors (which can

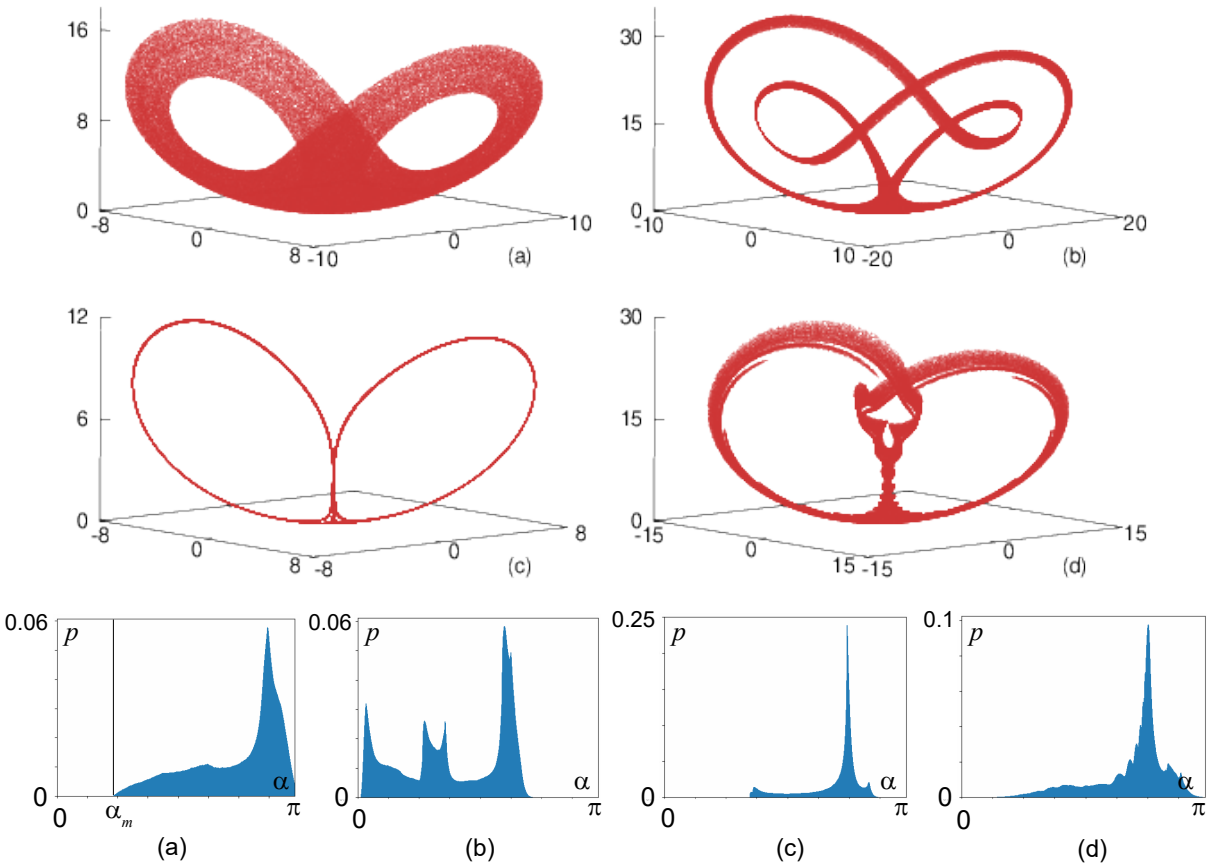

Figure 5: Pseudohyperbolic attractors for the map (1) for $\delta = 0.1$ found in: (a) region I, $(\rho, \sigma) = (8, 4)$, $\Lambda_1 = 0.02272, \Lambda_2 = 0, \Lambda_3 = -0.7692, \alpha_m = 0.39651$; (b) region II, $(\rho, \sigma) = (12.9, 2.3)$, $\Lambda_1 = 0.02265, \Lambda_2 = -0.00133, \Lambda_3 = -0.4613, \alpha_m = 0.017$; (c) region III, $(\rho, \sigma) = (6.25, 7)$, $\Lambda_1 = 0.01438, \Lambda_2 = -0.00624, \Lambda_3 = -1.54353, \alpha_m = 0.56488$; (d) region IV, $(\rho, \sigma) = (9.2, 8)$, $\Lambda_1 = 0.11218, \Lambda_2 = -0.08998, \Lambda_3 = -1.86316, \alpha_m = 0.1808$. In the bottom row histograms of angles between E^{ss} and E^{cu} are shown, these diagrams confirm the pseudohyperbolicity of the observed attractors.

appear only in maps).[3] Examples of attractors from these four regions are shown in Fig. 5. In the bottom row of this figure, we show histograms of the angles between E^{ss} and E^{cu}. These graphs confirm that the minimal angle α_m is separated from 0 for all these four attractors.

4 Kneading diagrams for discrete Lorenz attractors

In contrast to the Lorenz attractor, its discrete analogue is wild [32], i.e., it contains the wild hyperbolic set with inevitable homoclinic and heteroclinic tangencies between stable and unstable manifolds of saddle orbits belonging to this set. The tangency for a given pair of orbits (or between invariant manifolds of the same orbit) generically does not persist under perturbations, but there is a tangency between the invariant manifolds of

[3]The existence of homoclinic genuinely-discrete attractors appears to have been predicted for the first time in [28]; their properties and scenarios of the appearance are interesting problems for future research.

another pair of orbits (or another tangency between the invariant manifold of the given orbit) inside the wild hyperbolic set [50].

In this section, we adapt the so-called *kneading diagrams* method to detect the bifurcation curves corresponding to homoclinic tangencies between $W^u(O)$ and $W^s(O)$ inside discrete flow-like Lorenz attractors in the map (4). For parameter regions with such pseudohyperbolic attractors, we show that after the splitting of any given tangency between $W^u(O)$ and $W^s(O)$, another tangency between these manifolds appears, i.e., the corresponding attractor is wild.

The theory of kneading invariants, as quantities uniquely describing the complex dynamics of a system that admits a symbolic description with two symbols, was introduced in [47, 48]. This quantity is a topological invariant for systems with a Lorenz attractor [21, 44–46, 54]. In [3, 66] the kneading diagrams method was proposed for the study of flow systems with Lorenz-like attractors. The essence of this method is to compute, for parameters on a given grid, a kneading sequence along the unstable separatrix $W^u(O)$ and, based on this sequence, assign a unique color to the corresponding pixel. This method helps to visualize the complex organization of the homoclinic bifurcation curves in systems with Lorenz-like attractors [3, 52, 53, 66].

At first, we recall how to compute a kneading sequence for a Lorenz-like flow. After this, we describe how to adapt this method for close-to-identity maps with discrete Lorenz-like attractors.

4.1 Kneading diagram for the Lorenz system (3)

To compute the kneading sequence one proceeds as follows, see [3, 66].

1. First consider an initial condition $p_0 = (x_0, y_0, z_0) \in W^{u,+}_{\text{loc}}(O)$, where $W^u_{\text{loc}}(O)$ denotes the local positive (starting with $x > 0$) branch of the unstable one-dimensional invariant manifold of the equilibrium point at the origin,

2. Fix a large enough value of $T > 0$ and use a numerical scheme to approximate the positive semi-orbit segment

$$\Gamma_T = \{\varphi^t(p_0), \quad 0 \le t \le T\},$$

   where φ^t denotes the flow defined by (3).

3. Compute the successive intersections of such orbit segment with the Poincaré section

$$\Sigma = \{\max |x(t)|\},$$

   where $\varphi^t(p_0) = (x(t), y(t), z(t))$.

4. Let $n_{\texttt{cross}}$ be the number of intersections of Γ_T with Σ and, for $0 \le i \le n_{\texttt{cross}}$, let $(x_i, y_i, z_i) \in \mathbb{R}^3 \cap \Sigma$ be the i-th intersection (following the natural order induced by the flow evolution) of Γ_T with Σ.

5. Then define $k_i = 1$ whenever $x_i > 0$ and $k_i = -1$ otherwise. The sequence $(k_1, \ldots, k_{n_{\texttt{cross}}})$ obtained is the so-called kneading sequence truncated to order $n_{\texttt{cross}}$.

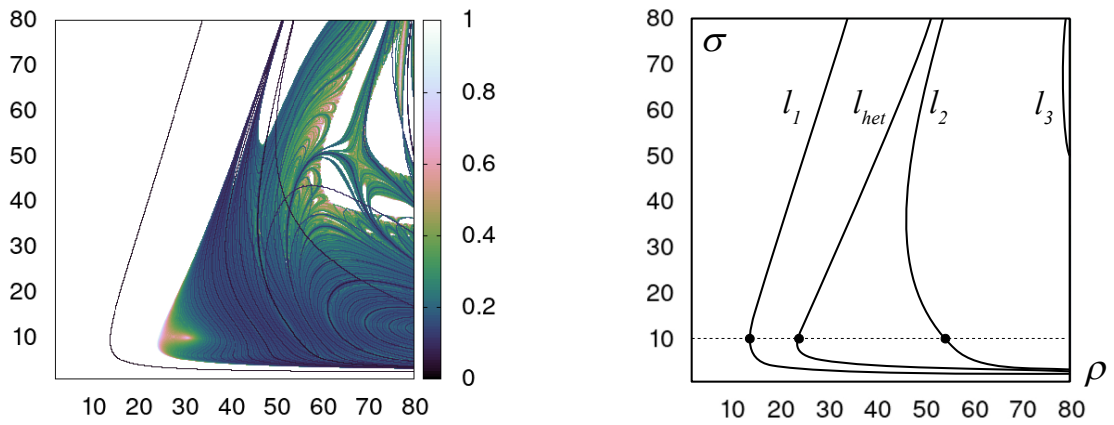

Figure 6: (a) Visualization of the kneading sequences for the Lorenz flow (3) as a function of the parameters ρ (horizontal axis) and σ (vertical axis); (b) Several bifurcation curves found in [10, 11, 60]: l_1, l_2, l_3 – 1-, 2-, and 3-round homoclinic orbits to the equilibrium O, l_{het} – heteroclinic bifurcation, see illustrations in Fig. 7

The previous simple procedure can be easily implemented to obtain the kneading sequences numerically.

In Fig. 6a, we present the results for the Lorenz flow (3) with $\beta = 8/3$. We use the following procedure to visualize the structure of the parameter space from the kneading sequences. Assume we have computed the kneading sequences (up to n_{max} kneading symbols, we use $n_{max} = 50$ symbols in our computations) for values on an equispaced mesh of parameters indexed by (i, j), where $1 \le i \le i_{max}$, $1 \le j \le j_{max}$. Denote by $k(i, j)$ the corresponding sequence and, let $n_{i,j}$ the number of coincident digits of $k(i, j)$ with its neighbors $k(i \pm 1, j)$ and $k(i, j \pm 1)$. We then display the corresponding values of the parameter using a color pattern chosen according to the normalized value of coincident symbols $n_{i,j}/n_{max}$.

Note that, using the previous visualization scheme, one can easily detect the homoclinic bifurcations of the equilibrium O that correspond to a change in one of the first symbols of the kneading. Hence, one can see the structure of the bifurcation curves in the parameter space in Fig. 6a.

The first curve, l_1, corresponds to the primary (1-round) homoclinic butterfly bifurcation, see Fig. 7a. On the curve l_{het}, which separates the colored region in Fig. 6a from the white one, there is a heteroclinic bifurcation: the unstable separatrices of O become lying on the stable invariant manifold of the pair of saddle periodic orbits which are born right after the homoclinic butterfly bifurcation, see Fig. 7b. After this bifurcation the chaotic attractor appears [60]. The curves l_2 and l_3 correspond to 2-round and 3-round homoclinic butterflies, see Figs. 7c-7d. A bifurcation diagram containing these curves was constructed in [60], see also [10, 11]. We have reproduced it with the help of the Matcont package [14] in Fig. 6b. A simple comparison of this diagram with the kneading diagram allows us to detect the curves $l_i, i = 1, 2, 3$ and l_{het} in Fig. 6a.

According to the Afraimovich, Bykov, Shilnikov theory [1, 2], homoclinic butterfly bifurcations are dense within the region containing Lorenz attractors. The nice foliated structure of the kneading diagram within the Lorenz attractor existence region (for its detection one can superimpose Fig. 4a with Fig. 6a) helps to visualize this result.

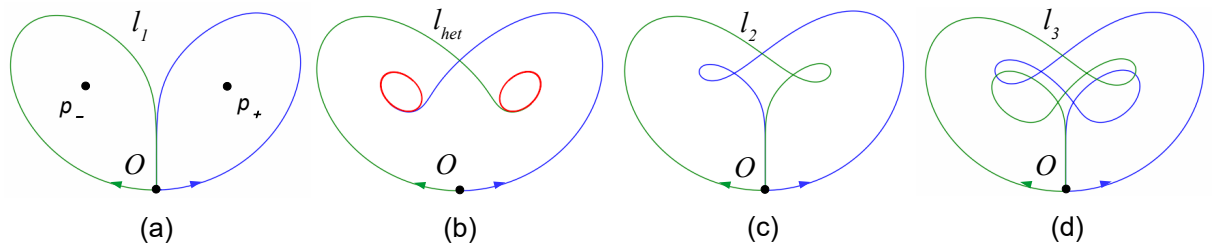

Figure 7: Phase portraits for homoclinic and heteroclinic bifurcations occurring on the curves: (a) l_1, (b) l_{het}, (c) l_2, (d) l_3. The portraits are shown for parameters marked by the bold points in Fig. 6b.

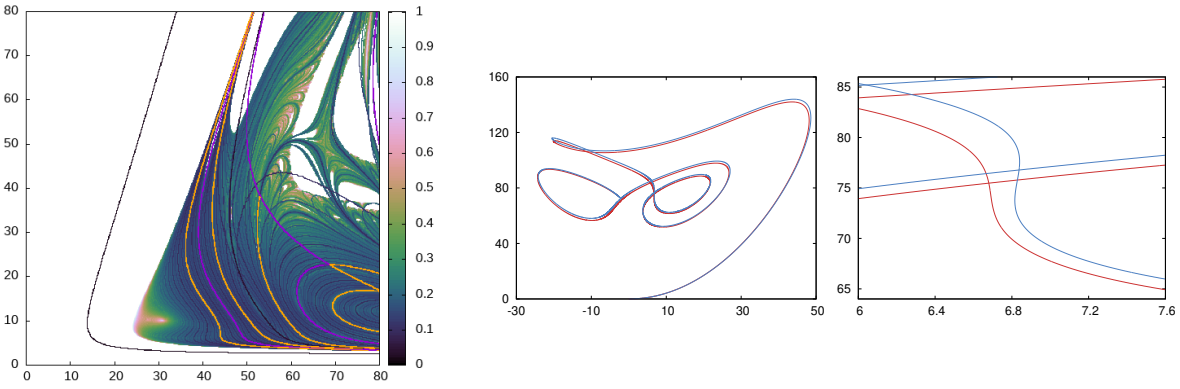

Figure 8: Left: On the kneading diagram for the Lorenz flow, we highlight different curves: the ones in purple (resp. in orange) correspond to a change in the sign of the 4th (resp. 5th) symbol in the kneading sequence. The center plot shows the (x, z)-coordinates of $W^{u,+}(O)$ for $\rho = 75.5$ (red) and $\rho = 76.5$ (blue). The right plot is a magnification of the center one showing that the blue line has a maximum of x near $(x, z) = (6.9, 79)$.

Remark 2 *The curves corresponding to homoclinic butterfly bifurcations are detected because crossing them produces a change in the sign of a symbol in the kneading sequence. However, not all detected curves correspond to homoclinic bifurcations of such type. For example, in Fig. 8a we superimpose the bifurcation curves where a change in the kneading sequence is detected at the 4th (purple) or 5th (orange) symbol. For* $\sigma = 18.9$*, at the crossing of the purple curve in the range* $\rho \in [61, 62]$ *there is a homoclinic butterfly bifurcation. But at the crossing of the orange curve taking place in* $\rho \in [75.5, 76.5]$*, a new maximum of* $|x|$ *along the separatrix gives an extra* 1 *in the 3rd position of the kneading sequence as shown in Figs. 8b-8c.*

Our further goal is to adapt the method of kneading diagrams for visualizing homoclinic bifurcations in discrete close-to-identity maps. The major difficulty in generalizing the previous scheme for a map is due to the transversal intersections of the invariant manifolds. In Fig. 9 we illustrate the situation for the map (4) near the first homoclinic bifurcation (an analogue of the primary homoclinic butterfly in the Lorenz flow). One can choose different points on a fundamental domain of the positive/negative branch of the invariant manifold, and the kneading symbols might differ drastically due to the oscillations observed in the figure. The oscillations are a consequence of the transversal intersection of the 1-dimensional unstable invariant manifold $W^u(O)$ with the 2-dimensional stable invariant manifolds $W^s(O)$.

In this work, we propose to approximate the corresponding kneading diagrams for

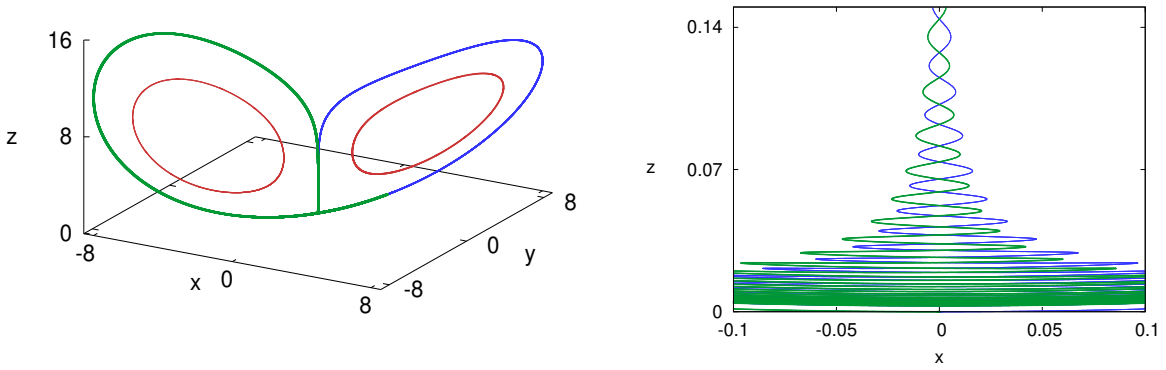

Figure 9: We consider the map (4) for $\delta = 0.075$, $\rho = 7.4559$, $\sigma = 10$ and $\beta = 8/3$. We display the one-dimensional unstable invariant manifold of the origin, $W^u(O)$ (the positive/negative branches are displayed in blue/green respectively). In the left plot, we also display the two attracting invariant curves (in red) observed for these values of the parameters. The right plot is a magnification of the left one, we see the two branches of the 1-dimensional invariant manifold $W^u(O)$ oscillating because they intersect the 2-dimensional stable manifold $W^s(O)$ (not displayed in the figure, but it roughly corresponds to the vertical line $x = 0$).

close-to-identity maps using the so-called interpolating vector fields (IVFs) [19].

4.2 Interpolating vector fields

Let us briefly recall the definition of IVFs given in [19]. Consider a smooth one-parameter near identity family of maps $F_\delta : D \to \mathbb{R}^m$ where $m \geq 1$, $D \subset \mathbb{R}^m$ is an open domain and $|\delta| < \delta_0$. It can be written as

$$F_\delta(x) = x + \delta\, G_\delta(x).$$

Fix $n \in \mathbb{N}$. Given $x \in D$, consider $x_k = F_\delta^k(x) \in D$ for $|k| \leq n$. Then, there exists a unique polynomial $p_n \in \mathcal{P}_{2n}(t)$ s.t. $x_k = p_n(t_k; x_0, \delta)$, for all $t_k = \delta k$ where $|k| \leq n$. The interpolating vector field (IVF) X_n at $x \in D$ is the velocity vector of the interpolating curve at $t = 0$, that is,

$$X_n(x, \delta) = \partial_t p_n(0, x, \delta).$$

Let us list some properties of the IVFs, see [19] for further details, proofs and examples of usage in a different setting:

1. X_n extends continuously to $\delta = 0$ and $X_n(x, 0) = G_0(x)$, that is, we recover the limit vector field.

2. The IVF X_n is a linear combination of the iterates of $x \in D$, concretely:

$$X_n(x, \delta) = \delta^{-1} \sum_{k=-n}^{n} p_{nk} x_k = \delta^{-1} \sum_{k=1}^{n} p_{nk}(x_k - x_{-k}),$$

where

$$p_{nk} = \frac{(-1)^{k+1}(n!)^2}{k(n+k)!(n-k)!}, \quad 1 \leq |k| \leq n.$$

3. A suspension of F_δ can be written as

$$Y(t,x,\delta) = A_n(x,\delta) + \delta^{2n} B_n(t,x,\delta)$$

where the $\mathcal{C}^{2n}$ norms of A_n and B_n are bounded uniformly with respect δ, then for every compact $D_0 \subset D$ there is a constant C_n such that

$$\sup_{x\in D} |A_n(x,\delta) - X_n(x,\delta)| \leq C_n \delta^{2n}$$

where X_n is the interpolating vector field for the map F_δ.

4. It follows from the previous item that, if $F_\delta \in \mathcal{C}^{2n+1}$ and $D_0 \subset D$ compact, then the IVF X_n is uniformly bounded in D_0 for $|\delta| < \delta_0$ and

$$F_\delta(x) = \Phi^\delta_{X_n}(x) + O(|\delta|^{2n+1}).$$

Below, we use IVFs to compute the kneading diagrams for a close-to-identity map. The results have been computed using IVF with $n = 5$. Note that if there is a Lorenz-like attractor for some parameters, then $W^u(O)$ is contained in a compact set $K \subset \mathbb{R}^3$. Assuming, for example, that the map (4) is $O(\delta)$-close to the identity map, then the IVF provides a uniform approximation of the dynamics of the map in K. Then, we consider the kneading sequence for the map as the kneading sequence for the IVF flow, which can be computed as it is usually done for a flow (see items 1-5 in Section 4.1).

4.3 IVF kneading sequences for the map (4)

First, we will show what happens with homoclinic structures (homoclinic butterflies) when we use IVF to compute kneading sequences. Consider again the map (4) for $\delta = 0.075$, $\sigma = 10$ and $\beta = 8/3$. We choose $\rho \in [7.4, 7.5]$ so that the homoclinic is expected to be created in this range. For values of ρ in this range, there is a transversal intersection of the unstable and stable invariant manifolds of the fixed point $O(0,0,0)$, as it is shown in Fig. 9. Our kneading computations reveal that the IVF has a homoclinic connection to the origin for $\rho = \rho_1 \in [7.4615, 7.462]$. The right branch of the invariant manifolds of O is displayed, for $\rho = 7.4615$ and $\rho = 7.462$, in Fig. 10. The kneading sequence is 1^∞ for $\rho < \rho_1$ and changes to $\{1, (-1)^\infty\}$ for $\rho > \rho_1$, in good agreement with Fig. 9.

On the other hand, the homoclinic connection (homoclinic butterfly) for the Lorenz flow (3) with $\sigma = 10$ and $\beta = 8/3$ takes place at $\rho \approx 13.926$. We have also shown that for the map with the same values of σ and β and with $\delta = 0.075$, there is a transversal intersection of $W^u(O)$ with $W^s(O)$ for $\rho \approx 7.45$, the value for which the IVF displays the homoclinic butterfly configuration. In Fig. 11 we display the results of the kneading computations for different values of ρ and δ. Notice that we recover the kneading sequences for the Lorenz flow as δ tends to zero. In particular, the homoclinic butterfly takes place along the bifurcation curve which tends to $\rho \approx 13.926$ when $\delta \to 0$, as expected.

Finally, we investigate the changes of the (ρ, σ)-parameter plane for different values of δ. The results are displayed in Fig. 12. The reader can see the similitude of the top left plot displayed for $\delta = 0.001$ with the kneading visualization in Fig. 6 for the Lorenz flow (3). Caution must be taken when interpreting the results for δ large because the IVF dynamics may differ from the real one since, for some parameters, the map may not be close enough to the identity in the whole region of interest containing the attractor.

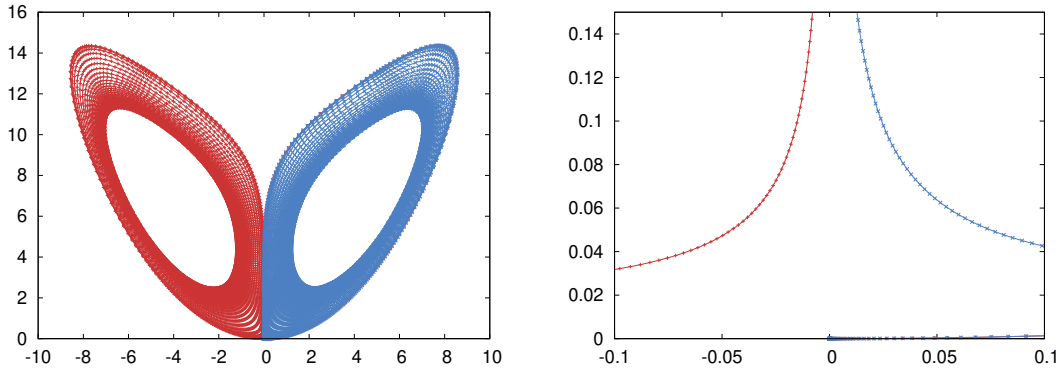

Figure 10: We display $W^{u,+}(O)$ for the IVF associated to the Lorenz map with $\delta = 0.075$, $\sigma = 10$ and $\beta = 8/3$, for $\rho = 7.4615$ (blue) and $\rho = 7.462$ (red). The right plot is a magnification of the left one where the detail of the trajectory at the passage near the saddle point at the origin is observed.

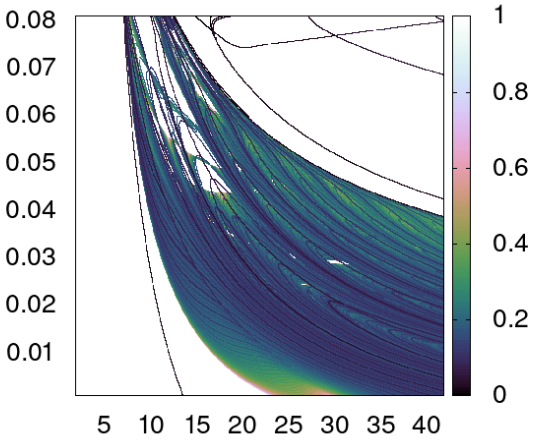

Figure 11: Bifurcation curves and (ρ, σ)-parameter structures revealed by IVF kneading sequences for the map (4) with $\sigma = 10$ and $\beta = 8/3$. We display the (ρ, δ)-parameter plane.

From Fig. 12 one can infer that the smooth foliation by homoclinic bifurcation curves of the parameter regions with pseudohyperbolic attractors (superimpose Figs. 4 with Figs. 12) persists even for relatively large values of δ. That is, homoclinic structures in the map (4) (analogous to the homoclinic butterflies in the Lorenz flow (3)) appear and disappear permanently with changes in parameter values. On the other hand, the appearance/disappearance of transversal homoclinic structures in maps occurs through the emergence of homoclinic tangencies. Thus, we can argue that homoclinic tangencies are inevitable inside the pseudohyperbolic attractors under consideration, i.e., these discrete Lorenz attractors are wild.

5 "1D Poincaré maps" from iterates of map (4)

As was already noticed by Lorenz in [40], the strong contraction in the normal directions to the attractor makes the successive intersections with $\Sigma_z = \{z = \rho - 1\}$ appear to fill a curve that resembles the graph of a 1D map. In particular, consider an initial point near O and let $p_k = (x_k, y_k, \rho - 1)$ be the k-th intersection of the corresponding orbit

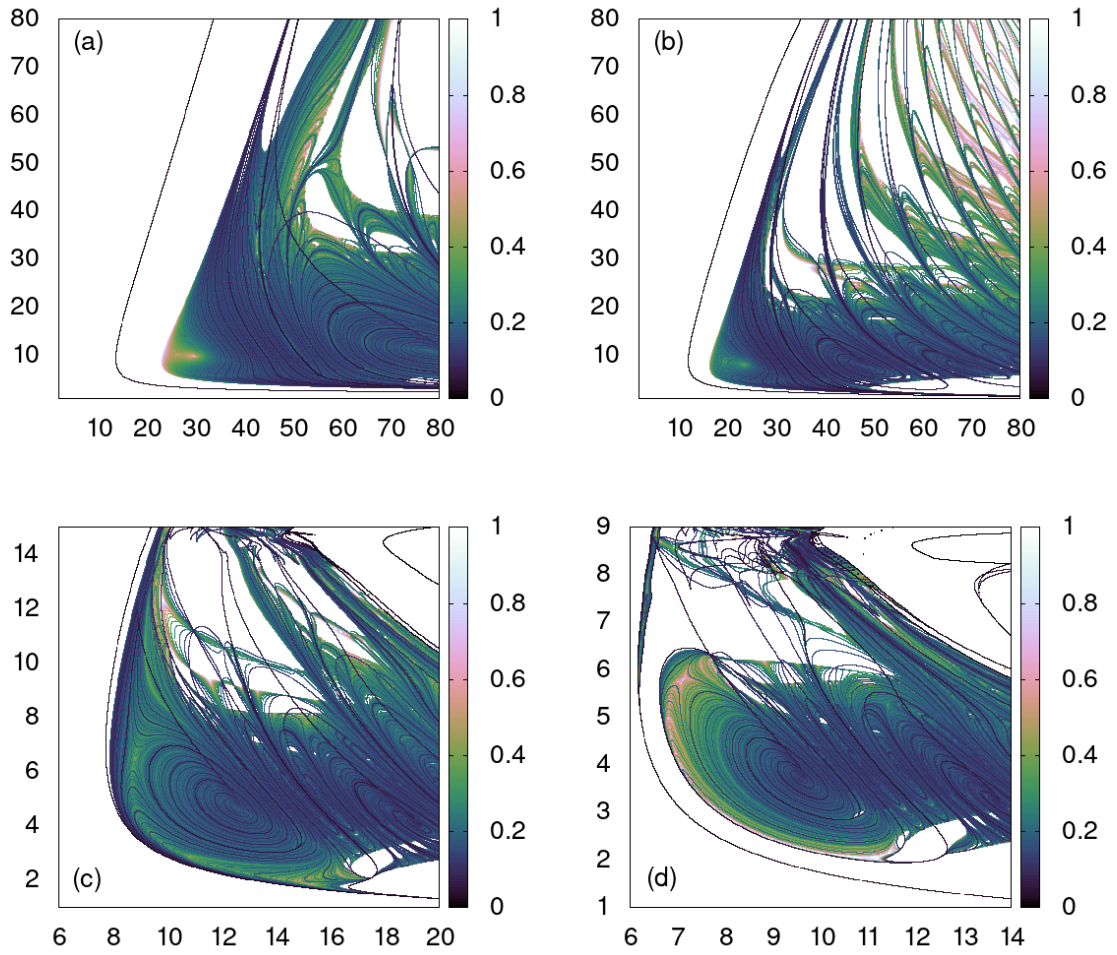

Figure 12: Bifurcation curves and (ρ, σ)-parameter structures revealed by IVF kneading sequences for the map (4) with $\beta = 8/3$ and (a) $\delta = 0.001$, (b) $\delta = 0.01$, (c) $\delta = 0.06$ and (d) $\delta = 0.1$.

with Σ_z. The locus of the set of points $(|x_k|, |x_{k+1}|)$ resembles a curve. For the classical parameters of the Lorenz attractor such a curve turns out to be similar to the graph of the tent map $f(x) = 2\min(x, 1-x)$. Changing parameters, when the attractor loses pseudohyperbolicity, said curve shows additional maxima and minima. Assuming that the curve is the graph of a 1D map, the presence of maxima/minima in the domain of the 1D map implies that such a map is no longer uniformly expansive [41, 42]. This is related to the existence of tangencies between E^{ss} and E^{cu}. In the following, we use this simple observation to check for the pseudohyperbolicity of the attractors for the Lorenz flow and the discrete Lorenz map.

Consider first the Lorenz flow (3) and an initial region of (ρ, σ) parameters. The computation of the first two kneading symbols allows us to discard those parameters on the left side of the curve l_1 in Fig. 6. For all the other parameters we integrate the system until $\texttt{nit}_0$ iterates of the Poincaré return map to $z = \rho - 1$ are obtained. Then we proceed as if there was a function $f : I \to I$, $I \subset \mathbb{R}$ an interval, such that $f(|x_k|) = |x_{k+1}|$ and we check if f has a minimum.

To proceed similarly for the map (4), we consider a point on the local unstable manifold of the origin and compute iterates until we cross Σ_z upwards (in the z-coordinate). Then

we integrate the flow of the IVF associated with the map (4) to compute a point on the (flow) Poincaré section Σ_z. Then, if $p_k = (x_k, y_k, \rho - 1) \in \Sigma_z$ denotes the k-th point obtained by the previous procedure, we display $|x_{k+1}|$ as a function of $|x_k|$ in Fig. 13. We see that, by projecting the iterates of the map onto Σ_z along the orbits of the IVF, the points (x_k,x_{k+1}) resemble a curve, so we will consider them as if they were on a graph of a function f, and we can proceed to check for minima of f. In other words, using IVF to project the iterates onto Σ_z the previous procedure can be applied provided δ is small enough.

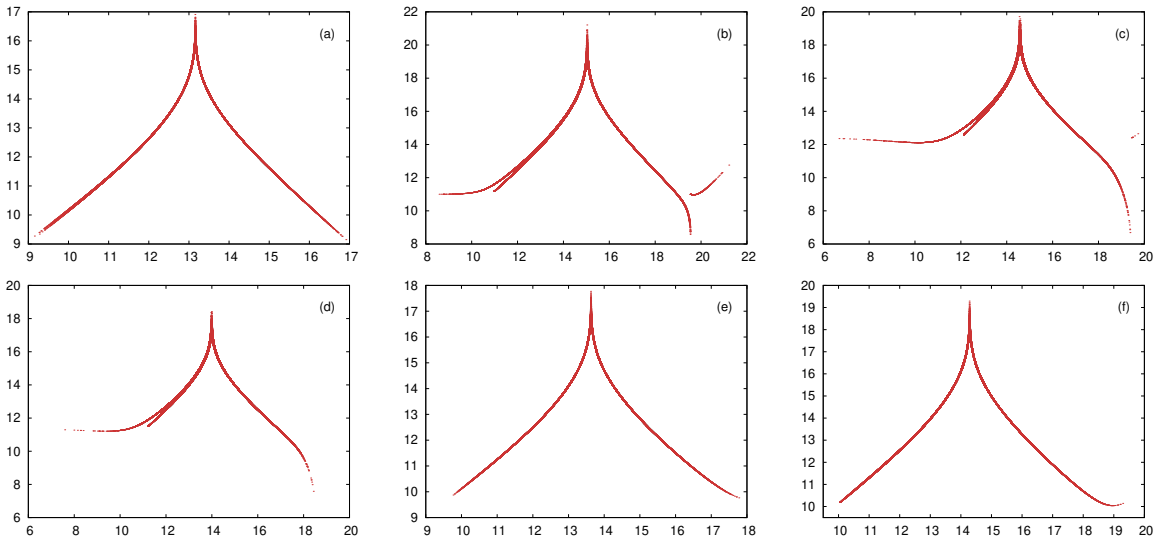

Figure 13: Iterates of the "1D maps" constructed using the IVF associated to map (4) for $\delta = 0.001$ and (ρ, σ) equals (a) (28,10), (b) (40,10), (c) (40,8), (d) (36,8), (e) (28,12) and (f) (32,12).

To check for minima we use the forward derivative formula to estimate f' from the obtained points in the section and we look for a change of the sign of the derivative f' in a range of $|x|$ where it is small (e.g. $< 10^{-5}$).

If, in this way, a "minimum" is detected (as happens for example in Fig. 13b, 13c, 13d and 13f) then we mark the attractor obtained for these parameters as non-pseudohyperbolic. Then, we repeat the computation for those parameters that remain candidates to be pseudohyperbolic by considering a larger number of iterates, $\texttt{nit} > \texttt{nit}_0$, of the Poincaré return map. The verification process can be iterated over the non-discarded points by making a larger number of iterates at each stage.

The results in Fig. 14 are obtained considering a grid with stepsize 5×10^{-2} in both parameters and $\texttt{nit} = 10^7$ iterates. The left plot shows the results for the Lorenz flow. The results for the map with $\delta = 0.01$ are displayed in Fig. 14b. In both cases, we display the region of parameters for which the pseudohyperbolicity of the attractor is not discarded. The curve l_A is shown for reference. This has been approximated by computing the minimal angle between the covariant Lyapunov vectors along $W^u(O)$, starting the forward propagation at an initial point close to O.

We conclude this section with some remarks regarding the algorithm and the results obtained:

- Regarding the results of the Lorenz flow, we note that the region bounded by the bifurcation curves l_{het}, shown in Fig. 6b and l_A, shown also in Fig. 4a, is well-

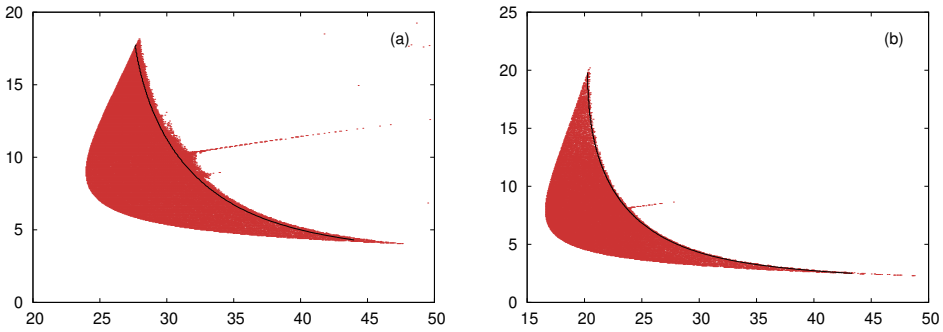

Figure 14: Parameter region where pseudohyperbolic attractors are expected for (a) the Lorenz flow, and (b) the map (4) with $\delta = 0.01$. The curve l_A is shown in black in both plots.

approximated by the region shown in Fig. 14a (where pseudohyperbolicity is not discarded). Refinements near l_A require a much larger number of iterates. For the map with $\delta = 10^{-2}$, the region is better approximated near the boundary curve l_A, as shown in the right plot.

- It is known that on the curve l_A there is a special configuration, called the principal T-point or Bykov point [7–9, 20], where $W^{u,+}(O)$ is a heteroclinic orbit to the equilibrium p_- (we denote as p_+/p_- the equilibrium points located in the right/left wings of the attractor, shown in Fig. 7a). It is known to be located at $(\rho, \sigma) \approx (30.8668, 10.1673)$, and it is clearly detected in the kneading diagram in Fig. 6. In Fig. 14a we observe what resembles a line emerging from the principal T-point to the right of the pseudohyperbolic region. This line was labeled as h_1 in [13] and parameters on this line correspond to homoclinic/heteroclinic connections of $p_\pm$. Interestingly, a similar curve is detected in the results for the map in Fig. 14b.

  The points near h_1 are not discarded in our procedure because, for parameters below the curve h_1, the minimum of f is located for values of $|x|$ near the maximum while, on the other hand, for parameters above the curve h_1, the minimum of f is detected near the minimum of $|x|$. For points on the curve, no minimum inside the domain of f is expected. This complicates the detection of the minimum of f when getting close to the curve h_1 since it approaches the boundary of the interval where f can be considered. With a much larger number of iterates, most of the points near h_1 will be discarded by the algorithm.

- For larger values of δ not all the "1D map" reductions obtained are satisfactory. First, as pointed out in Section 3, the fact that the map is no longer close enough to the identity leads to genuinely-discrete attractors. On the other hand, large values of δ create attractors similar to butterfly homoclinic attractors but that return to O with a spiraling behavior around the z-axis, see Fig. 5d and Fig. 15a for illustrations. The corresponding "1D map" does not resemble a graph of a tent-like function, see Fig. 15b, hence invalidating the procedure described in this section to check pseudohyperbolicity.

  Note however that the flow attractor of the IVF, shown in Fig. 15c, resembles the

discrete attractor, shown in Fig. 15a. The corresponding 1D map reduction obtained from direct integration of the IVF is shown in Fig. 15d. Here we see that such a flow attractor is not pseudohyperbolic. Although probably δ is too large to have any justified relation, we note that this agrees with the results based on minimal angle computations (the point $(\rho, \sigma) = (14, 12)$ is colored in dark blue in Fig. 4c).

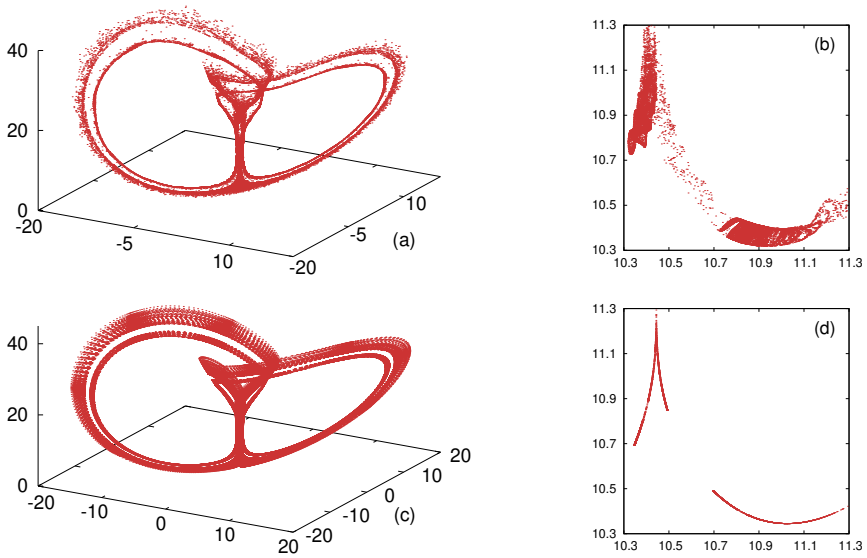

Figure 15: We consider $\delta = 0.06$, $\beta = 8/3$, $\rho = 14$ and $\sigma = 12$. Figures (a) and (b) are obtained from iterates of the map (4) while figures (c) and (d) are obtained by integration of the IVF. The right plots (b) and (d) display $2 \cdot 10^4$ successive iterates of the Poincaré map of a point lying on the corresponding (left plot) attractor.

6 Conclusions and future research directions

In this paper, we have studied a family of close-to-identity maps that display a rich variety of discrete Lorenz-like attractors. Explorations based on Lyapunov exponents and minimal angle computations illustrate this richness. The fact that the family of maps recovers the Lorenz flow as the step parameters tend to zero allowed us to use interpolating vector fields (IVFs) to generalize for maps (and systematically check by comparison with the flow) some of the usual algorithms for flows. In particular, we have shown how to obtain kneading diagrams to detect bifurcation curves for the map and how to reduce the dynamics to "1D Poincaré" maps. These generalizations require a small enough step parameter. Otherwise, genuinely-discrete attractors might appear as have also illustrated.

Future research directions include exploring the applicability of the tools used in this work for the study of discrete Lorenz attractors in various systems of interest in applications like the Celtic stone model [22] or the model of thermosolutal convection [16]. In particular, it will be interesting to investigate if, using IVFs, we can verify the pseudohyperbolicity of the attractors which is quite difficult to do with the help of the angle method due to additional first integrals in the models.

On the other hand, near the codimension three point with multipliers $(-1, -1, 1)$, the second iterate of the Hénon map (1) is close to the identity and then IVFs can provide

some insights on the structure of the attractors that are created at such a bifurcation.

As a final comment, we believe that the fact that IVFs are explicitly obtained from iterates of the map might be useful to mathematically formalize the ideas here sketched. For example, complemented with accurate analytic bounds, IVFs might be useful to generalize the Afraimovich-Bykov-Shilnikov geometric model for the case of close-to-identity maps.

Acknowledgements

A.V. and A.M. have been supported by the Spanish grant PID2021-125535NB-I00 (MICINN/AEI/FEDER, UE) and the Catalan grant 2021-SGR-01072. A.V. also acknowledges the Severo Ochoa and María de Maeztu Program for Centers and Units of Excellence in R&D (CEX2020-001084-M). A.K. has been supported by the Laboratory of Dynamical Systems and Applications NRU HSE, the grant of the Ministry of Science and higher education of the RF, ag. № 075-15-2022-1101. The work of K.Z. has been supported by the RSF grant No. 19-71-10048.

References

[1] V. S. Afraimovich, V. Bykov, and L. P. Shilnikov. "On the origin and structure of the Lorenz attractor". In: *Akademiia Nauk SSSR Doklady* 234 (1977), pp. 336–339.

[2] V. S. Afraimovich, V. Bykov, and L. P. Shilnikov. "Attractive nonrough limit sets of Lorenz-attractor type". In: *Trudy Moskovskoe Matematicheskoe Obshchestvo* 44 (1982), pp. 150–212.

[3] R. Barrio, F. Blesa, S. Serrano, and A. Shilnikov. "Global organization of spiral structures in biparameter space of dissipative systems with Shilnikov saddle-foci". In: *Physical Review E* 84.3 (2011), p. 035201.

[4] R. Barrio, A. Shilnikov, and L. Shilnikov. "Kneadings, symbolic dynamics and painting Lorenz chaos". In: *International Journal of Bifurcation and Chaos* 22.04 (2012), p. 1230016.

[5] D. Barros, C. Bonatti, and M. J. Pacifico. "Up, down, two-sided Lorenz attractor, collisions, merging and switching". In: *arXiv preprint arXiv:2101.07391* (2021).

[6] G. Benettin, L. Galgani, A. Giorgilli, and J.-M. Strelcyn. "Lyapunov characteristic exponents for smooth dynamical systems and for Hamiltonian systems; a method for computing all of them. Part 1: Theory". In: *Meccanica* 15.1 (1980), pp. 9–20.

[7] V. Bykov. "On the generation of a non-trivial hyperbolic set from a contour formed by separatrices of saddles". In: *Methods of the Qualitative Theory of Differential Equations*. Gorky Univ. Press Gorky, 1988, pp. 22–32.

[8] V. Bykov. "The bifurcations of separatrix contours and chaos". In: *Physica D: Nonlinear Phenomena* 62.1-4 (1993), pp. 290–299.

[9] V. Bykov. "The generation of periodic motions from the separatrix contour of a three-dimensional system". In: *Uspekhi Matematicheskikh Nauk* 32.6 (1977), pp. 213–214.

[10] V. Bykov and A. Shilnikov. "On the boundaries of the domain of existence of the Lorenz attractor". In: *Methods of Qualitative Theory and Theory of Bifurcations. Gorky State University, Gorky* (1989), pp. 151–159.

[11] V. Bykov and A. Shilnikov. "On the boundaries of the domain of existence of the Lorenz attractor". In: *Selecta Mathematica Sovietica* 1.4 (1992), pp. 375–382.

[12] M. J. Capiński, D. Turaev, and P. Zgliczyński. "Computer assisted proof of the existence of the Lorenz attractor in the Shimizu–Morioka system". In: *Nonlinearity* 31.12 (2018), p. 5410.

[13] J. L. Creaser, B. Krauskopf, and H. M. Osinga. "Finding first foliation tangencies in the Lorenz system". In: *SIAM Journal on Applied Dynamical Systems* 16.4 (2017), pp. 2127–2164.

[14] A. Dhooge, W. Govaerts, Y. A. Kuznetsov, H. G. E. Meijer, and B. Sautois. "New features of the software MatCont for bifurcation analysis of dynamical systems". In: *Mathematical and Computer Modelling of Dynamical Systems* 14.2 (2008), pp. 147–175.

[15] J. Eilertsen and J. Magnan. "On the chaotic dynamics associated with the center manifold equations of double-diffusive convection near a codimension-four bifurcation point at moderate thermal Rayleigh number". In: *International Journal of Bifurcation and Chaos* 28.08 (2018), p. 1850094.

[16] J. S. Eilertsen and J. F. Magnan. "Asymptotically exact codimension-four dynamics and bifurcations in two-dimensional thermosolutal convection at high thermal Rayleigh number: Chaos from a quasi-periodic homoclinic explosion and quasi-periodic intermittency". In: *Physica D: Nonlinear Phenomena* 382 (2018), pp. 1–21.

[17] N. Gavrilov and L. Shilnikov. "On three-dimensional dynamical systems close to systems with a structurally unstable homoclinic curve. I". In: *Mathematics of the USSR-Sbornik* 17.4 (1972), p. 467.

[18] N. Gavrilov and L. Shilnikov. "On three-dimensional dynamical systems close to systems with a structurally unstable homoclinic curve. II". In: *Mathematics of the USSR-Sbornik* 19.1 (1973), p. 139.

[19] V. Gelfreich and A. Vieiro. "Interpolating vector fields for near identity maps and averaging". In: *Nonlinearity* 31.9 (2018), pp. 4263–4289.

[20] P. Glendinning and C. Sparrow. "T-points: a codimension two heteroclinic bifurcation". In: *J. Statist. Phys.* 43.3-4 (1986), pp. 479–488.

[21] P. Glendinning and C. Sparrow. "Prime and renormalisable kneading invariants and the dynamics of expanding Lorenz maps". In: *Physica D: Nonlinear Phenomena* 62.1-4 (1993), pp. 22–50.

[22] A. S. Gonchenko, S. V. Gonchenko, and A. O. Kazakov. "Richness of chaotic dynamics in nonholonomic models of a Celtic stone". In: *Regular and Chaotic Dynamics* 18.5 (2013), pp. 521–538.

[23] A. S. Gonchenko, S. V. Gonchenko, A. O. Kazakov, and A. Kozlov. "Elements of contemporary theory of dynamical chaos: A tutorial. Part I. Pseudohyperbolic attractors". In: *International Journal of Bifurcation and Chaos* 28.11 (2018), p. 1830036.

[24] A. Gonchenko and E. Samylina. “On the region of existence of a discrete Lorenz attractor in the nonholonomic model of a Celtic stone”. In: *Radiophysics and Quantum Electronics* 62 (2019), pp. 369–384.

[25] S. Gonchenko, M. Kainov, A. Kazakov, and D. Turaev. “On methods for verification of the pseudohyperbolicity of strange attractors”. In: *Izvestiya VUZ. Applied Nonlinear Dynamics* 29.1 (2021), pp. 160–185.

[26] S. V. Gonchenko, D. V. Turaev, and L. P. Shilnikov. “Dynamical phenomena in multidimensional systems with a structurally unstable homoclinic Poincaré curve”. In: *Doklady Akademii Nauk* 330.2 (1993), pp. 144–147.

[27] S. V. Gonchenko, D. V. Turaev, and L. P. Shilnikov. “On the existence of Newhouse regions in a neighborhood of systems with a structurally unstable homoclinic Poincaré curve (the multidimensional case)”. In: *Doklady Akademii Nauk* 329.4 (1993), pp. 404–407.

[28] S. Gonchenko and A. Gonchenko. “On discrete Lorenz-like attractors in three-dimensional maps with axial symmetry”. In: *Chaos: An Interdisciplinary Journal of Nonlinear Science* 33.To appear (2023).

[29] S. Gonchenko, A. Gonchenko, A. Kazakov, and E. Samylina. “On discrete Lorenz-like attractors”. In: *Chaos: An Interdisciplinary Journal of Nonlinear Science* 31.2 (2021), p. 023117.

[30] S. Gonchenko, E. Karatetskaia, A. Kazakov, and V. Kruglov. “Conjoined Lorenz twins—a new pseudohyperbolic attractor in three-dimensional maps and flows”. In: *Chaos: An Interdisciplinary Journal of Nonlinear Science* 32.12 (2022).

[31] S. Gonchenko, A. Kazakov, and D. Turaev. “Wild pseudohyperbolic attractor in a four-dimensional Lorenz system”. In: *Nonlinearity* 34.4 (2021), pp. 2018–2047.

[32] S. V. Gonchenko, I. I. Ovsyannikov, C. Simó, and D. Turaev. “Three-dimensional Hénon-like maps and wild Lorenz-like attractors”. In: *International Journal of Bifurcation and Chaos* 15.11 (2005), pp. 3493–3508.

[33] S. V. Gonchenko, L. P. Shilnikov, and D. V. Turaev. “On dynamical properties of multidimensional diffeomorphisms from Newhouse regions: I”. In: *Nonlinearity* 21.5 (2008), p. 923.

[34] S. Gonchenko, A. Gonchenko, I. Ovsyannikov, and D. Turaev. “Examples of Lorenz-like attractors in Hénon-like maps”. In: *Mathematical Modelling of Natural Phenomena* 8.5 (2013), pp. 48–70.

[35] S. Gonchenko, L. Shilnikov, and D. Turaev. “Dynamical phenomena in systems with structurally unstable Poincaré homoclinic orbits”. In: *Chaos: An Interdisciplinary Journal of Nonlinear Science* 6.1 (1996), pp. 15–31.

[36] J. Guckenheimer. “A strange, strange attractor, The Hopf bifurcation and its applications”. In: *The Hopf bifurcation and its applications*. Vol. 19. Springer-Vedlag, 1976, pp. 368–381.

[37] J. Guckenheimer and R. F. Williams. “Structural stability of Lorenz attractors”. In: *Publications Mathématiques de l’IHÉS* 50 (1979), pp. 59–72.

[38] P. V. Kuptsov. “Fast numerical test of hyperbolic chaos”. In: *Physical Review E* 85.1 (2012), p. 015203.

[39] P. V. Kuptsov and S. P. Kuznetsov. "Lyapunov analysis of strange pseudohyperbolic attractors: angles between tangent subspaces, local volume expansion and contraction". In: *Regular and Chaotic Dynamics* 23.7 (2018), pp. 908–932.

[40] E. N. Lorenz. "Deterministic nonperiodic flow". In: *J. Atmospheric Sci.* 20.2 (1963), pp. 130–141.

[41] S. Luzzatto and W. Tucker. "Non-uniformly expanding dynamics in maps with singularities and criticalities". In: *Inst. Hautes Études Sci. Publ. Math.* 89 (1999), pp. 179–226.

[42] S. Luzzatto and M. Viana. "Positive Lyapunov exponents for Lorenz-like families with criticalities". In: 261. Géométrie complexe et systèmes dynamiques (Orsay, 1995). 2000, pp. xiii, 201–237.

[43] D. Lyubimov and M. Zaks. "Two mechanisms of the transition to chaos in finite-dimensional models of convection". In: *Physica D: Nonlinear Phenomena* 9.1-2 (1983), pp. 52–64.

[44] M. Malkin. "Periodic orbits, entropy, and rotation sets of continuous mappings of the circle". In: *Ukrainian Mathematical Journal* 35.3 (1983), pp. 280–285.

[45] M. Malkin. "Rotation intervals and dynamics of Lorenz-like maps". In: *Methods of Qualitative Theory of Differntial Equations* (1985), pp. 122–139.

[46] M. Malkin. "Rotation intervals and the dynamics of Lorenz type mappings". In: *Selecta Mathematica Sovietica* 10.3 (1991), pp. 265–275.

[47] J. Milnor and R. Thurston. "On iterated maps of the interval". In: (1977).

[48] J. Milnor and W. Thurston. "On iterated maps of the interval". In: *Lecture notes in mathematics* 1342 (1988), pp. 465–563.

[49] C. A. Morales, M. J. Pacifico, and E. R. Pujals. "Robust transitive singular sets for 3-flows are partially hyperbolic attractors or repellers". In: *Annals of mathematics* (2004), pp. 375–432.

[50] S. E. Newhouse. "The abundance of wild hyperbolic sets and non-smooth stable sets for diffeomorphisms". In: *Publications Mathématiques de l'IHÉS* 50 (1979), pp. 101–151.

[51] I. I. Ovsyannikov and D. Turaev. "Analytic proof of the existence of the Lorenz attractor in the extended Lorenz model". In: *Nonlinearity* 30.1 (2016), p. 115.

[52] K. Pusuluri, H. G. Meijer, and A. L. Shilnikov. "Homoclinic puzzles and chaos in a nonlinear laser model". In: *Communications in Nonlinear Science and Numerical Simulation* 93 (2021), p. 105503.

[53] K. Pusuluri and A. Shilnikov. "Homoclinic chaos and its organization in a nonlinear optics model". In: *Physical Review E* 98.4 (2018), p. 040202.

[54] D. Rand. "The topological classification of Lorenz attractors". In: *Mathematical Proceedings of the Cambridge Philosophical Society*. Vol. 83. 3. Cambridge University Press. 1978, pp. 451–460.

[55] A. M. Rucklidge. "Chaos in models of double convection". In: *Journal of Fluid Mechanics* 237 (1992), pp. 209–229.

[56] A. Shilnikov. "Bifurcation and chaos in the Morioka-Shimizu system". In: *Selecta Math. Soviet* 10.2 (1991), pp. 105–117.

[57] A. Shilnikov. "Bifurcations and chaos in the Shimizu–Marioka system". In: *in Methods and Qualitative Theory of Differential Equations, Gorky State University* (1986), pp. 180–193.

[58] A. Shilnikov, L. Shilnikov, and D. Turaev. "Normal forms and Lorenz attractors". In: *International Journal of Bifurcation and Chaos* 3.05 (1993), pp. 1123–1139.

[59] A. L. Shilnikov. "On bifurcations of the Lorenz attractor in the Shimizu-Morioka model". In: *Physica D: Nonlinear Phenomena* 62.1-4 (1993), pp. 338–346.

[60] L. Shilnikov. "Bifurcation theory and the Lorenz model". In: *Appendix to Russian edition of "The Hopf Bifurcation and Its Applications." Eds. J. Marsden and M. McCraken* (1980), pp. 317–335.

[61] J. C. Tatjer. "Three-dimensional dissipative diffeomorphisms with homoclinic tangencies". In: *Ergodic Theory Dynam. Systems* 21.1 (2001), pp. 249–302.

[62] W. Tucker. "The Lorenz attractor exists". In: *Comptes Rendus de l'Académie des Sciences-Series I-Mathematics* 328.12 (1999), pp. 1197–1202.

[63] D. V. Turaev and L. P. Shilnikov. "An example of a wild strange attractor". In: *Sbornik: Mathematics* 189.2 (1998), p. 291.

[64] D. Turaev and L. Shilnikov. "Pseudohyperbolicity and the problem on periodic perturbations of Lorenz-type attractors". In: *Doklady Mathematics* 77.1 (2008), p. 17.

[65] R. F. Williams. "The structure of Lorenz attractors". In: *Publications Mathematiques de l'IHES* 50 (1979), pp. 73–99.

[66] T. Xing, R. Barrio, and A. Shilnikov. "Symbolic quest into homoclinic chaos". In: *International Journal of Bifurcation and Chaos* 24.08 (2014), pp. 1440004, 20.